

# **Study of Topological Phenomena Through Berry Phase in Classical Nonlinear Elastic Granules**

Kazi T. Mahmood & M. Arif Hasan\*

Department of Mechanical Engineering, Wayne State University, Detroit, MI 48202

[kazi.tahsin.mahmood@wayne.edu](mailto:kazi.tahsin.mahmood@wayne.edu), [hasan.arif@wayne.edu](mailto:hasan.arif@wayne.edu)

## **Abstract**

The geometric or Berry phase concept, traditionally rooted in quantum mechanics, has been found to be increasingly significant in classical mechanics, particularly for understanding the dynamics of linear and nonlinear systems. In this study, we demonstrate the controlled accumulation of the Berry phase in a classical system using a two-level time-dependent elastic bit, analogous to a quantum bit, within a nonlinear environment generated by a two-granular network. The nonlinearity of the granular beads is modulated through the frequency and amplitude of external harmonic excitation, along with static preloading. By employing the orthonormal basis of the nonlinear responses and mapping the displacement coefficients in Bloch states, we reveal how time influences the manipulation of the elastic bit and its states. Our analytical and experimental investigations uncover the Berry phase's role in revealing various topological characteristics of the classical granular network. This research establishes a crucial link between classical and quantum realms via the Berry phase of an elastic bit, with significant implications for decoherence-free and robust data transfer and information processing.

## Introduction

Exploration of geometric and Berry phases has introduced a new area of research in both quantum and classical domains. The geometric phases are generated in adiabatic cyclic processes, offering a profound understanding of the dynamics of the physical systems. The geometric phase depends on the global properties of the system rather than the path it follows, which is necessary to define the topology [1]. This shows the essence of the topological property for the geometric phase and can be utilized for quantum computation and information processing. The Berry phase is the topological interpretation of the geometric phase [2]. Various fields have utilized the topological nature of the berry phases, showing decoherence-free operations of qubits and unique electrical operation of topological insulators through non-trivial topology [3-6]. Berry phase observation can also be used in classical mechanics, which extends beyond quantum mechanics [7-9]. Topology defines system structures and functionality by describing how system components are arranged and interlinked. Comprehending topological structures is essential for the bulk-edge correspondence principle, which projects localized states at the boundary of crystals of varying topologies, facilitating decoherence-free one-way information transmission [10]. Recent studies have shown the Berry phase's effect in topological computing by realizing the non-Abelian braiding, Majorana encoding, and non-holonomic computing [11-14]. The Berry phase depends on the global and non-integrable paths, making it suitable for disturbance-free energy transmission [15].

The study of the Berry phase has gained momentum in one-level systems like harmonic oscillators and superlattices and two-level classical systems like elastic bits or phi bits [16, 17]. Studies have shown the accumulation of the geometric phase in the topological elastic oscillations, vibrations, and waves, representing a one-level system [18]. These studies represent manipulating the Berry phases through the internal parameters of the system. In contrast, later studies have developed the two-level system of the elastic bit where the berry phase accumulation in a linearized granular system is manipulated by external excitation, like amplitude, frequency, and the phase difference between the drivers [19]. However, the study of the Berry phase in a nonlinear network, where the coherent states have time dependency, and a single excitation shows multiple superpositions of states through time, still needs to be explored.

The research on topological characteristics in nonlinear classical mechanics has opened new dimensions of understanding the complex dynamical behaviors across various physical systems. Several recent studies have found theoretical and numerical evidence of nonlinear traveling edge waves in a two-dimensional weakly nonlinear phononic topological insulator and other related nonlinear phononic structures [20-22]. Notably, these topological effects are evident in granular crystals, a nonlinear elastic metamaterial type. Given the fundamental nonlinearities in these media, the elastic waves are highly tunable and adaptive to various applied excitations and static preloading [23]. Strong precompression renders the system slightly nonlinear, whereas no precompression renders the system very nonlinear. Recent studies have demonstrated that a specific arrangement of ordered granular beads can mimic certain quantum behaviors like superpositions of states and entanglement in a classical setting by forming an elastic bit [24, 25].

The current study focuses on generating the Berry phase in a harmonically driven nonlinear granular system, where the coherent states are time-dependent, as a nonlinear system is required to unveil the true quantum phenomena. Previous studies have theoretically and experimentally established the classical analogue of the qubit, elastic bit, through coupled granular bead network and harmonizing the system [23, 26]. The external excitation manipulates the response of the

granules, and by tuning the amplitude, frequency, and phase, we explore a multitude of nonlinear responses. Here, a nonlinear solution is observed to measure the quantum-like phenomena by the power expansion of the forces. This creates eigenstates providing the in-phase and out-of-phase for the elastic system. We use these orthonormal bases of those amplitudes to calculate the single elastic bit's state by demonstrating the Bloch sphere. The Bloch sphere is the geometrical demonstration of the state of a quantum system where the polar and azimuthal angles are the basis of the system's state [27]. We use numerical and experimental approaches to validate our theoretical study. We will show how the amplitude and phases of the granules at the characteristic frequency of the nonlinear modes can influence the Berry phase. This opens the possibility of topology-based mass sensing by manipulating granules through external excitation.

The study establishes the approach of the accumulation of the Berry phase in a sequence of theoretical study and experimental approaches. In section 2, we develop the mathematical modeling necessary for forming the elastic bit, and the Bloch states to show the effect of the external excitation in the accumulation of the Berry phase. In section 3, we compare our theoretical approach with the numerical simulation for higher-order nonlinearity in the system. In section 4, we create an experimental procedure to see the effect of the external excitation on the Berry phase.

### Theoretical Formulation of the Berry Phase in a Nonlinear Granular Network

In this section, we create a mathematical model to calculate the Berry Phase of nonlinear granular networks by representing the network through elastic bits in a two-level coherent superposition of states and mapping the elastic bits in the Bloch sphere. The two-level network consists of two elastically coupled granules connected in a single point contact. Section 2.1 shows the displacement time response of the granules due to the external excitation through the perturbation theory and the multitude of the amplitude of the granules. Section 2.2 shows the formation of the elastic bit from the displacement vector and illustrates its Bloch states. Lastly, section 2.3 demonstrates the accumulation of the time-dependent periodic Berry phase and their dependency on external excitation and static preloading.

#### 2.1 Mathematical Modeling:

The general mathematical formulation for the nonlinear granular network can be expressed through the displacement and force [28]. We do the Taylor series expansion of the displacement field and taking till the third order stiffness, we can get the displacement field as (Detailed Derivation at the Supplementary Material),

$$\begin{aligned}
m\ddot{u}_1 &= \left[ k_1(F_1 e^{i\omega_D t} - u_1) + k_2(F_1 e^{i\omega_D t} - u_1)^2 + k_3(F_1 e^{i\omega_D t} - u_1)^3 + \dots \right]_+ \\
&\quad - \left[ k_1(u_1 - u_2) + k_2(u_1 - u_2)^2 + k_3(u_1 - u_2)^3 + \dots \right]_+ - \eta\dot{u}_1 \\
m\ddot{u}_2 &= - \left[ k_1(u_2 - F_2 e^{i\omega_D t}) + k_2(u_2 - F_2 e^{i\omega_D t})^2 + k_3(u_2 - F_2 e^{i\omega_D t})^3 + \dots \right]_+ \\
&\quad + \left[ k_1(u_1 - u_2) + k_2(u_1 - u_2)^2 + k_3(u_1 - u_2)^3 + \dots \right]_+ - \eta\dot{u}_2
\end{aligned} \tag{1}$$

Here,  $u_1$  are the  $u_2$  are the displacement of the granules from the equilibrium.  $m$  is the mass of the granules, which depends on the shape and materials of the granules.  $k_1 = \frac{3}{2} k_{NL} \delta_0^{\frac{1}{2}}$ ,  $k_2 = -\frac{3}{8} k_{NL} \delta_0^{-\frac{1}{2}}$ ,  $k_3 = -\frac{3}{48} k_{NL} \delta_0^{-\frac{3}{2}}$  are the different order coupling stiffness for the granular beads and  $k_{NL}$  depends on the mechanical properties of the granules.  $\delta_0$  represents the static precompression on the granules.  $F_1$  and  $F_2$  represents the magnitude of the external harmonic excitation and  $\omega_D$  is the frequency. We use a multi-order perturbation technique to find the approximate solution of the

granular network. The solutions of the system are assumed as  $u_1 = u_{1,0} + \epsilon u_{1,1} + \epsilon^2 u_{1,2} + \dots$  and  $u_2 = u_{2,0} + \epsilon u_{2,1} + \epsilon^2 u_{2,2} + \dots$ . Here,  $\epsilon$  represents the order of the stiffness between the coupling. And  $u_{1,m}$  and  $u_{2,m}$  represents the order of the displacement due to the higher order of stiffness. The system's viscous damping reacts to the movement of the granules, with the adjustment made to the viscous damping due to the drag between the air and the granules.

We place the assumed solution of  $u_1$  and  $u_2$  in Eq. (1) to get the multi-order vibration response for the granules with respect to  $\epsilon$ . We equate the order of stiffness coefficients  $\epsilon$  to get the different order of displacement  $u_{1,m}$  and  $u_{2,m}$ . For the two granules, we get,

First Granule		(2)
$\epsilon^0$	$m\ddot{u}_{1,0} = k_1[(F_1 e^{i\omega_D t} - u_{1,0}) - (u_{1,0} - u_{2,0})] - \eta\dot{u}_{1,0}$	
$\epsilon^1$	$m\ddot{u}_{1,1} = k_1[(-u_{1,1}) - (u_{1,1} - u_{2,1})] + k_2[(F_1 e^{i\omega_D t} - u_{1,0})^2 - (u_{1,0} - u_{2,0})^2] - \eta\dot{u}_{1,1}$	
$\epsilon^2$	$m\ddot{u}_{1,2} = k_1[(-u_{1,2}) - (u_{1,2} - u_{2,2})] + k_2(-2F_1 e^{i\omega_D t} u_{1,1} + 2u_{1,0} u_{1,1}) - k_2(2u_{1,0} u_{1,1} - 2u_{1,1} u_{2,0} - 2u_{1,0} u_{2,1} + 2u_{2,0} u_{2,1}) + k_3[(F_1 e^{i\omega_D t} - u_{1,0})^3 - (u_{1,0} - u_{2,0})^3] - \eta\dot{u}_{1,2}$	
Second Granule		
$\epsilon^0$	$m\ddot{u}_{2,0} = k_1[(u_{1,0} - u_{2,0}) - (u_{2,0} - F_2 e^{i\omega_D t})] - \eta\dot{u}_{2,0}$	
$\epsilon^1$	$m\ddot{u}_{2,1} = k_1[(u_{1,2} - u_{2,2}) - (u_{1,2})] + k_2[(u_{1,0} - u_{2,0})^2 - (u_{2,0} - F_2 e^{i\omega_D t})^2] - \eta\dot{u}_{2,1}$	
$\epsilon^2$	$m\ddot{u}_{2,2} = k_1[(u_{1,2} - u_{2,2}) - (u_{1,2})] + k_2(2F_2 e^{i\omega_D t} u_{2,1} - 2u_{2,0} u_{2,1}) + k_2(2u_{1,0} u_{1,1} - 2u_{1,1} u_{2,0} - 2u_{1,0} u_{2,1} + 2u_{2,0} u_{2,1}) + k_3[(u_{1,0} - u_{2,0})^3 - (u_{2,0} - F_2 e^{i\omega_D t})^3] - \eta\dot{u}_{2,2}$	

The amplitude of the nonlinear vibration has a different order, as in the case of displacement. And the amplitudes have their own characteristic frequencies. Using the method of undetermined coefficients, we get amplitudes as,

$u_{1,0} = A_{1,0} e^{i\omega_D t}$	$u_{2,0} = A_{2,0} e^{i\omega_D t}$	(3)
$u_{1,1} = 2A_{1,1} e^{2i\omega_D t}$	$u_{2,1} = 2A_{2,1} e^{2i\omega_D t}$	
$u_{1,2} = 3A_{1,2} e^{3i\omega_D t}$	$u_{2,2} = 3A_{2,2} e^{3i\omega_D t}$	

Here  $A_{1,m}$  and  $A_{2,m}$  are the multi-order amplitudes at the different characteristic frequencies of the vibrating granules. As we have multiple amplitudes due to the perturbation of the dynamic equations of the granular network, we can have a nonlinear response based on the order of the expansion of the equations.

## 2.2. Study of the Classical Coherent Superposition of States:

Now as we establish the multi-order amplitudes of the nonlinear granular network, we investigate the orthonormal basis of the amplitudes of the granules. In this section, we will discuss the formation of the elastic bit from the amplitude of the granules, with the realization of the complex amplitude coefficients. The displacement field resembles the effect of the eigenstates of the system. To understand the eigenstates of the nonlinear system, we focus on the single harmonic mode of vibration. In the case of a single amplitude, when the precompression of the system is higher and  $k_2$  and  $k_3$  are negligible, the system is considered a linearized system because only

zeroth order amplitude is present. The vibrational responses of the granules are defined through the eigenstates of  $E_1$  and  $E_2$ . The  $E_1$  and  $E_2$  states are the corresponding in-phase and out-of-phase eigenmodes for a linearized granular system. If the phase difference between the granules is 0, the system is described by the state  $E_1 = \frac{1}{\sqrt{2}} \begin{pmatrix} 1 \\ 1 \end{pmatrix}$  (in-phase mode), and if the phase difference between the granules is  $\pi$ , the system is described by the state  $E_2 = \frac{1}{\sqrt{2}} \begin{pmatrix} 1 \\ -1 \end{pmatrix}$  (out-of-phase mode). Any other phase difference between the granules defines the combination of both eigenstates.

The combinations of  $E_1$  and  $E_2$  form a complete orthonormal basis for the granular network despite the absence of the orthogonality property of the nonlinear modes. So, we can form a basis for the states of the granular system in the form of  $E_1$  and  $E_2$ . The coefficients at each of the characteristic frequencies correspond to the superposed states, which can have characteristics of phase difference of in-phase and out-of-phase mode or in-between. We define these coherent states such that  $E_1$  and  $E_2$  have constant phases and show interference for an instant of time. Over time, the coherent state stays coherent, but its phase relation evolves, stating the time dependency of the superposed states' overall coefficients. Therefore, we use the analogy of the quantum system, Dirac notations for vectors, and apply them to the elastic states. Hence, the total displacement field has a complex time-dependent coefficient (See Supplementary Materials for detail).  $\tilde{\alpha}(t)$  and  $\tilde{\beta}(t)$ , which can be expressed as,

$$\vec{U} = \begin{pmatrix} u_1 \\ u_2 \end{pmatrix} = \sum_{n=1} \begin{pmatrix} A_{1,n-1} \\ A_{2,n-1} \end{pmatrix} e^{ni\omega_n t} \equiv \frac{1}{\sqrt{|\tilde{\alpha}(t)|^2 + |\tilde{\beta}(t)|^2}} [\tilde{\alpha}(t)|E_1\rangle + \tilde{\beta}(t)|E_2\rangle] \quad (4)$$

Here,  $\tilde{\alpha}(t) = \left( \sum_n \frac{1}{\sqrt{|\alpha_n|^2 + |\beta_n|^2}} \alpha_n e^{ni\omega_n t} \right)$  and  $\tilde{\beta}(t) = \left( \sum_n \frac{1}{\sqrt{|\alpha_n|^2 + |\beta_n|^2}} \beta_n e^{ni\omega_n t} \right)$ .  $\alpha_n$  and  $\beta_n$  are the complex amplitude coefficients stating the orthonormal basis at the characteristic frequency of the displacement field. And  $n = 1, 2, \dots$  are the  $n^{th}$  complex amplitudes of the  $n^{th}$  dominant characteristic frequency. The two mutually orthogonal eigenstates  $E_1$  and  $E_2$  form an orthonormal basis, which can be described as Hilbert space. Nonlinearity allows the states to evolve in the Hilbert space through time as the coefficients are time-dependent.

This coherent time-dependent superposition of states can be visualized in a 3-dimensional geometric space through the geometrical representation of the Bloch sphere. Each elastic bit is a vector in the Bloch sphere and mapped in the Bloch states. And these vectors have two components: polar angle  $\theta$  and azimuthal angle  $\varphi$ . As we are defining the coherent states in the Bloch sphere if the coherent superposition of states  $\tilde{\alpha}$  and  $\tilde{\beta}$  are time-dependent, so as  $\tilde{\theta}$  and  $\tilde{\varphi}$ . The Bloch sphere also represents the orthogonal eigenstates that depend on  $\tilde{\theta}(t)$  and  $\tilde{\varphi}(t)$  as  $\tilde{\alpha}(t)$  and  $\tilde{\beta}(t)$ . The modal contribution to the overall displacement field's mode superposition can be expressed as a column displacement vector.  $|\psi\rangle$  [23, 26] (Detail in Supplementary Material).

$$|\psi\rangle = \begin{pmatrix} \tilde{\alpha}(t) \\ \tilde{\beta}(t) \end{pmatrix} = \begin{pmatrix} \cos \frac{\tilde{\theta}(t)}{2} \\ e^{i\tilde{\varphi}(t)} \sin \frac{\tilde{\theta}(t)}{2} \end{pmatrix} \quad (5)$$

The argument of the column displacement vector  $|\psi\rangle$  obtained through the Bloch sphere component describes the geometric phase of the granules. At the pure states for the elastic bit and

the polar angle  $\tilde{\theta}$  are referring to the phase difference  $\phi_{u_1-u_2}$  between the granules, while the azimuthal angle  $\tilde{\varphi}$  demonstrate the evolution of the states in the Bloch sphere [19].

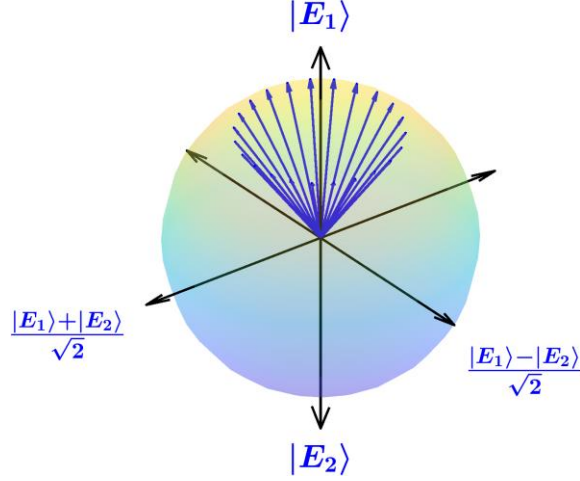


**Figure 1:** Effect of nonlinearity on the modulus and the Bloch sphere angle of the superposition of states complex coefficients for the precompression  $\delta_0 = 0.7$  with the driving frequency of  $\omega_D = 1.366$ , and the force of the drivers at  $F_1 = 1, F_2 = 1.5$ , the viscous damping is  $\eta = 0.3$ . It shows the evolution in the Bloch states when the polar angle  $\tilde{\theta}$  has low variation, and the azimuthal angle completes  $2\pi$  revolution.

Figure 1 represents the evolution of states in a Bloch sphere for a particular driving condition. This driving condition shows that the azimuthal angle  $\tilde{\varphi}$  creates complete  $2\pi$  revolution. Also, it creates a small variation of the polar angle  $\tilde{\theta}$  over time, and the mean value of  $\tilde{\theta}$  is  $\frac{\pi}{6}$ . This condition shows that the states revolve around the pure state  $E_1$ . The smaller variation of  $\tilde{\theta}$  also allows the calculation of the Berry phase using classical theory  $\gamma = \frac{1}{2}(\tilde{\varphi}_f - \tilde{\varphi}_i)(1 - \cos \tilde{\theta}_{mean})$ . This is comparable to the phase accumulation of the Foucault pendulum, which shows the relation of the classical system to the quantum analogous system [29]. The nonlinear responses allow the states to explore more regions of the Bloch sphere rather than a single plane, like a linearized system [19]. We can manipulate this movement by changing the applied excitation and precompression. This manipulation is important, as it shows the formation of the elastic bit like the topological qubit. We can show the elastic bit's classical effect as the Berry phase's accumulation. Berry phase is a global phase, which depends on the global properties of the path taken in the parameter space, not on the local perturbations. This gives the elastic bit robustness, which is susceptible to decoherence. The coherent states can be the basis of topological computing, which will be discussed later. In the later section, we will also show the Berry phase accumulation due to the higher variation of the polar angle  $\tilde{\theta}$  and revolution of the azimuthal angle  $\tilde{\varphi}$  other than  $2\pi$ .

### 2.3. Berry Phase in a nonlinear system:

The mapping of the coherent superposition of states in the Bloch sphere is manipulated through the external driver. This shows that we can control the formation of the elastic bit. The manipulation creates a specific Berry phase, which depends on the evolution of the polar and azimuthal angle. Previous approaches have shown that the Berry connection can be defined by the variation of the complex amplitude vectors parametrized by wave number [30, 31], and summing the Berry connection for the wave number over the closed path gives Berry phase [2, 32]. Later, for the linearized coupled network, it was shown that the Berry connection can be evaluated concerning Bloch sphere angle  $\theta$  and  $\varphi$  [19]., summing the Berry connection for the wave number

over the closed path gives Berry phase [2, 32]. Later, for the linearized coupled network, it was shown that the Berry connection can be evaluated concerning Bloch sphere angle  $\theta$  and  $\varphi$  [19, 30, 31], and summing the Berry connection for the wave number over the closed path gives Berry phase [2, 32]. Later, for the linearized coupled network, it was shown that the Berry connection can be evaluated concerning Bloch sphere angle  $\theta$  and  $\varphi$  [19]. While these studies have discretized the space through the variation of the external excitation and the manipulation of internal parameters, a nonlinear granule network can create this discretized parametric space through time for a specific external excitation. The Berry connection in the parametric space of time with the relation of time-dependent Bloch sphere angles  $\tilde{\theta}(t)$  and  $\tilde{\varphi}(t)$ , we can write,

$$BC(\tilde{\theta}(t), \tilde{\varphi}(t)) = \frac{1}{2} \left[ \left( \cos \frac{\tilde{\theta}(t)}{2} + e^{i\tilde{\varphi}(t)} \sin \frac{\tilde{\theta}(t)}{2} \right)^* \cdot \left( \cos \frac{\tilde{\theta}(t+\Delta t)}{2} + e^{i\tilde{\varphi}(t+\Delta t)} \sin \frac{\tilde{\theta}(t+\Delta t)}{2} \right) + \left( \cos \frac{\tilde{\theta}(t)}{2} - e^{i\tilde{\varphi}(t)} \sin \frac{\tilde{\theta}(t)}{2} \right)^* \cdot \left( \cos \frac{\tilde{\theta}(t+\Delta t)}{2} - e^{i\tilde{\varphi}(t+\Delta t)} \sin \frac{\tilde{\theta}(t+\Delta t)}{2} \right) \right] \quad (6)$$

Here, the berry connection is discretized over time, which characterizes the variation in the orientation of the unit vector along some path in a complex space of coefficient parameters along that time. Previous studies showed the accumulation of the Berry phase in a cyclic environment where the initial parameters of the unit vector are re-achieved over the closed discretized parametric space [33]. We use Eq. (6) to calculate the Berry phase accumulated over time in cyclic and noncyclic environments where the closed parametric space is not required. By the manipulation of the external excitation, we can create both closed and open loops of the azimuthal angle of  $\tilde{\varphi}(t)$ . A  $2\pi$  revolution of  $\tilde{\varphi}$  states a closed loop or any other angle states the open loop. In any case, the Berry phase associated with the berry connection is the product of the connection in the parametric space of time [2, 34]. We get,

$$\gamma = -\frac{1}{N} \text{Im} \left[ \sum \left( \ln \left( BC \left( \tilde{\theta}(t), \tilde{\varphi}(t) \right) \right) \right) \right] \quad (7)$$

Here,  $N$  represents the number of periods taken for the Berry phase to accumulate. As in Eq. (7), the Berry phase is the net phase accumulated over the external excitation frequency, and the berry connection is spanned across the response period. Each period accumulates a particular Berry phase, adding to the increased total period. Thus, we can say that the Berry phase characterizes the topology of the elastic bit.

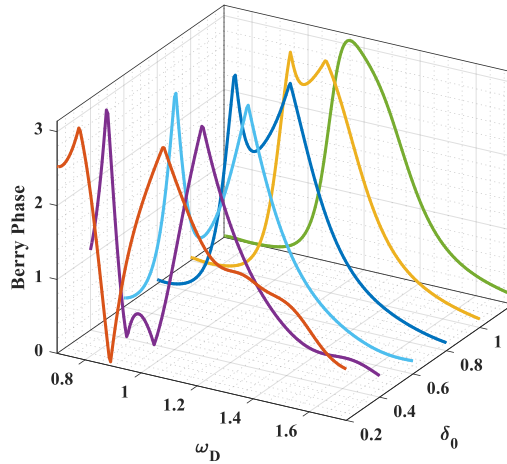


**Figure 2:** Evolution of the Berry phase in the nonlinear granular medium due to the external excitation of the granules. Applying static precompression can change the Berry phase formation at different forces and frequencies. System Parameters:  $F_1 = 1$ ,  $F_2 = 2.5$ , and  $\eta = 0.4$ .

Figure 2 demonstrates how Berry phase values vary between 0 and  $\pi$  in response to changes in the frequencies ( $\omega_D$ ) of external drivers and the applied static precompression ( $\delta_0$ ). At a lower precompression when the system is nonlinear, there are two instances when the Berry phase attains a non-trivial value of  $\pi$ , even for a fixed precompression value. Observing two identical non-trivial berry phases indicates the system might have similar vibrational modes at different driving frequency conditions in the nonlinear regime. This contrasts with the findings by Jayaprakash et al., where the authors showed the different families of NNMs and subharmonic orbits modes of the two-granule system in the frequency-energy plot [35]. The authors noted families of two NNMs and subharmonic orbits defined over the entire energy range. From Fig. 2, we also observe a trivial berry phase of 0 between the two non-trivial Berry phases. If the value of the static precompression increases, i.e., if we move towards the weakly nonlinear regime, the two non-trivial berry phase values come closer and move to higher frequencies.

Further, with the increase of precompression, the observance of the trivial berry phase value of 0 vanishes, which was observed before in between the non-trivial berry phases. At very high precompression, when the system is close to the linearized regime, the two non-trivial Berry phases merge into one and display one non-trivial berry phase as we sweep the driving frequency. Thus, Fig 2 demonstrates the interplay between the extrinsic driver parameters and the intrinsic precompression parameters to achieve the non-trivial Berry phase of  $\pi$ . Altering the driving frequency allows tuning the static precompression to reach the same non-trivial Berry phase of  $\pi$ . It is important to note that the occurrence of a non-trivial Berry phase of  $\pi$  depends not only on the driving frequency but also on the drivers' amplitude since the system is nonlinear. Such findings highlight the elastic bit's versatility in producing any Berry phase values, including trivial and non-trivial, typically associated with integral multiples of  $\pi$ . Such findings are crucial to realize topological analogue computing that relies on the Berry phase.

Such findings are crucial to realize topological analogue computing that relies on the Berry phase. One of the building blocks for topological computing is braiding. When two elastic bits are braided around each other, the system undergoes a unitary transformation that can be used to perform quantum gates. The exchange of elastic bits results in a specific Berry phase that depends on the path taken during the exchange, leading to non-trivial braiding [11]. This braiding can perform quantum analogue gates that are inherently fault-tolerant due to their topological nature [14].

The findings are also important for realizing the Majorana encoding. Majorana zero modes provide a way to encode qubits non-locally. A pair of Majorana modes can represent a single elastic bit, with the elastic bit state being defined by the parity of the fermion number shared between the modes. The Berry phase arising from the exchange (braiding) of these modes ensures that the elastic bit's state is determined by the global properties of the braid, not by local disturbances [12].

Another field of study of the Berry phase is in non-Holonomic computing, which depends on the non-Holonomic dynamics. Non-holonomic systems are those whose state evolution depends on non-integrable constraints, meaning the constraints cannot be expressed solely in terms of the system's coordinates [13]. These constraints typically involve relationships between the system's position and its derivatives, leading to path-dependent behavior. Path-dependent non-holonomic systems can implement time-dependent coherent states, resulting in a decoherent and robust computing network.



### Numerical Study of the Granular Network:

We proceed to demonstrate the numerical analysis of the two-mass nonlinear granular system. Numerical analysis provides a deeper understanding of the nonlinear granules. We have constructed a discrete element model to study the berry phase of the elastic bit formed by these beads; this type of discrete element model has been used extensively in the literature on granular media [36, 37].

The numerical calculations take effect of the higher order of stiffness for the displacement field. Setting the initial condition for the granules as,  $u_n = 0$  we can formulate the nonlinear equation for the two-mass granular network [23]. By applying the external excitation through the amplitude and frequency and static preloading on the masses, we reveal the multi-order harmonic response of the granules. The displacement field is later mapped onto the orthonormal basis with the combination of  $E_1$  and  $E_2$  to calculate the complex amplitude coefficients  $\tilde{\alpha}$  and  $\tilde{\beta}$ . Later, the coefficients are mapped onto the Bloch sphere through the polar ( $\tilde{\theta}$ ) and azimuthal ( $\tilde{\varphi}$ ) angle. The  $\tilde{\theta}$  and  $\tilde{\varphi}$  can be formulated for the Berry curvature using Eq. (6) and for the Berry phase using Eq. (7). Using a similar driving condition to the theoretical study, we can see the effect on the elastic bit in the numerical study.

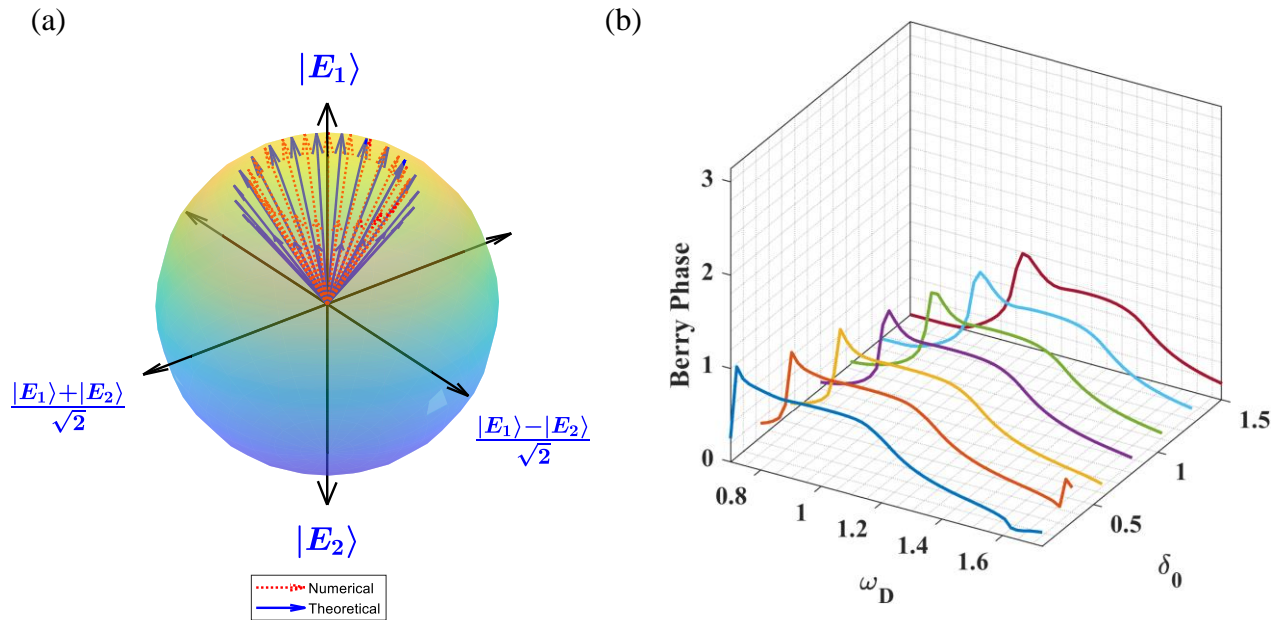


**Figure 3:** Numerical calculation of the nonlinear granular beads from Eq. (1), and the berry phase calculation of numerical Bloch states using Eq. (6) and (7), (a) the numerical Bloch sphere depicting the consistency of the theoretical calculations. System parameters:  $F_1 = 1$ ,  $F_2 = 1.5$ ,  $\delta_0 = 0.7$  and  $\eta = 0.3$ . (b) Evolution of the Berry phase due to the numerical analysis of the coupled granular network. System Parameter:  $F_1 = 1$ ,  $F_2 = 2.5$  and  $\eta = 0.4$ .

Figure 3 shows the analysis of the Bloch states and Berry phases using the numerical simulation of the generalized nonlinear granular network equation. Using similar driving conditions, the evolution of the states is visualized in the Bloch sphere, along with the comparison with the theoretical study in Fig. 3(a). The azimuthal angle  $\tilde{\varphi}$  also shows a complete  $2\pi$  revolution in this condition. And the polar angle  $\tilde{\theta}$  has a small variation over time, and the mean of  $\tilde{\theta}$  is 0.49. The Berry phase calculated through Eq. (6) and (7) is comparable with the theoretical study  $\gamma_{theo} =$

0.41, where we can see the Berry phase for the numerical study  $\gamma_{num} = 0.37$ . Figure 3(b) shows the Berry phase change at a particular driving condition by changing the frequency and the precompression in the numerical calculations. At lower precompression  $\delta_0$ , the higher quantity of Berry phase reveals at a lower frequency. With the increase of  $\delta_0$ , the higher value of Berry phase shifts to higher frequencies. Although the trivial Berry phase of 0 is present, the non-trivial Berry phase of  $\pi$  is absent. This is different from theoretical study. Because of the change of the amplitude and phase at the characteristic frequencies and higher order of vibrations than the theoretical study, the Berry phase shows different responses in the case of the numerical study.

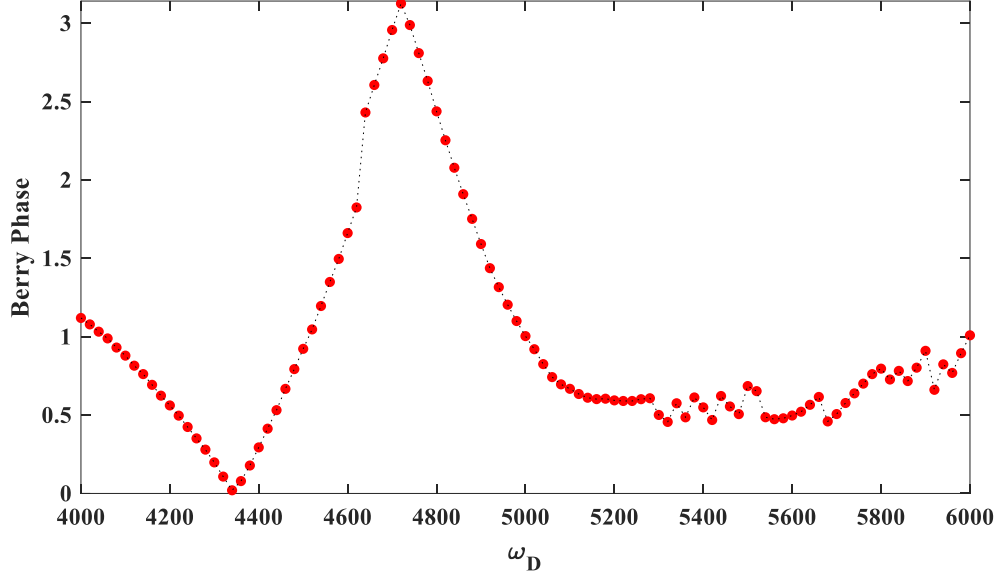
Using the third-order nonlinear terms, we find the vibrating amplitudes of the granules,  $A_{1,m}$  and  $A_{2,m}$ . We can see the effect of the amplitudes at the trivial and non-trivial Berry phases. Different Berry phase regions formulize the peak-to-peak ratio at the characteristic frequency amplitudes. For different amplitude relationships of  $A_{n,0}/A_{n,1}$ , and  $A_{n,1}/A_{n,2}$ , we can find different berry phases for manipulating the external excitation.

The numerical analysis shows the dependency of the coherent states and berry phase on the vibrational response of the granules. As the responses are consistent over time, this indicates the robustness of the elastic bits as the coherent states are also attained at each period. This makes the system more compliant with topological computing. The braiding of the elastic bits is done with time, making it a path dependent tool for non-Holonomic computing.

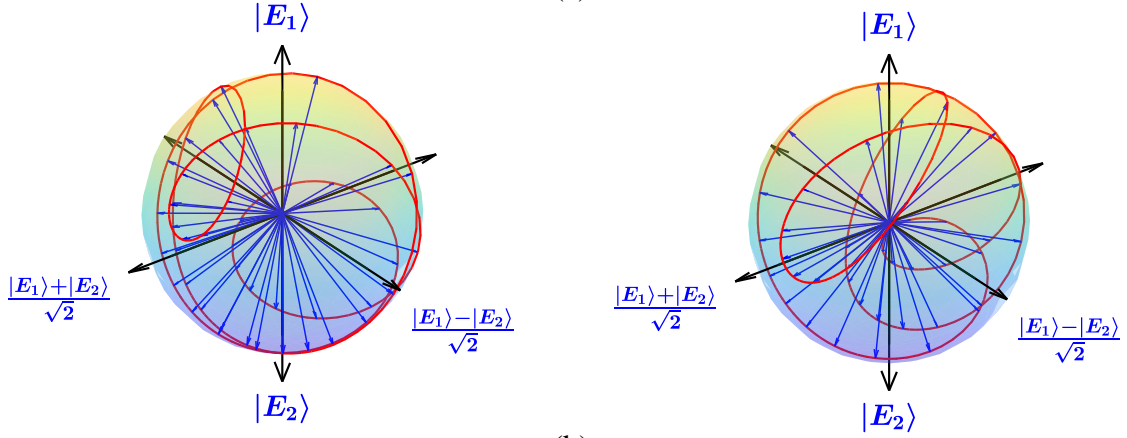
### **EXPERIMENTAL REALIZATION OF THE GRANULE SYSTEM:**

In this experimental procedure, we excite only one mass in the two-mass granular network. As in the previous studies, we can see the nonlinear responses by driving one of the granular beads; we implement the frequency at one granule to create the time-dependent elastic bit. To realize the nature of the elastic bit system comprised of the granular beads, we explore the elastic wave in the form of the time series. Like the procedure of theoretical and numerical modeling, using the orthonormal basis of the elastic bit, we can map the amplitude at those characteristics' frequencies at the coherent states, and from there, we get the time-dependent complex amplitude coefficient  $\tilde{\alpha}$  and  $\tilde{\beta}$ . After that, by mapping the coherent states, we can get the Bloch states through the time-dependent polar ( $\tilde{\theta}$ ) and azimuthal angle ( $\tilde{\varphi}$ ). We visualize the Berry phase of the system through the Bloch states to correlate with the vibrational response of the granules.

We can see the evolution of the Berry phase at different frequencies, keeping the amplitude of the driver the same, stating the effect of external excitation on the granular beads, which forms the trivial and non-trivial Berry phases and a combination of both.



(a)



(b)

**Figure 4:** Demonstration of the Berry phase generation at different frequencies of the nonlinear response of the granular beads and the condition of the superposition of states at the trivial and non-trivial Berry phase. (a) The change of the Berry phase calculated through both open and closed loop conditions due to frequency change at amplitude  $A = 120 V_{p-p}$ . (b) and (c) Measurement of the response of the two-mass granule elastic system at frequency: Left Panel:  $\omega_D = 4340 \text{ Hz}$  and Right Panel:  $\omega_D = 4720 \text{ Hz}$  with the amplitude  $A = 120 V_{p-p}$ . (b) the phase difference of the dominant amplitudes at characteristic frequency stating the combination of the eigenstate of  $E_1$  and  $E_2$ .

Figure 4 shows the evolution of the Berry phase experimentally at different driving frequencies, driving one of the granules, and the evolution of states in the trivial and non-trivial Berry phase. Figure 4(a) represents the Berry phase accumulation at each period at different frequencies and the change of the Berry phase from trivial (0) to non-trivial ( $\pi$ ). At the driving frequency of  $\omega_D = 4340 \text{ Hz}$ , we can see the accumulation of trivial Berry phase of 0. And at the driving frequency of  $\omega_D = 4720 \text{ Hz}$ , the non-trivial Berry phase of  $\pi$  is accumulated over the period. We can find other Berry phase accumulation at other frequencies rather than the trivial and non-trivial Berry phase. Figure 4(b) shows the evolution of the states in a Bloch sphere at the frequencies of trivial and non-trivial Berry phases. In the left panel, when the Berry phase is 0, the states are seen to be

completing multiple twists with time. In the case of the right panel, when the Berry phase is  $\pi$ , we can see more twists than the other case along time. This shows the effect of nonlinearity in the accumulation of the Berry phase in the elastic bit generated due to the vibration of the granules. The Berry phase experimentally demonstrated depends on the amplitude and phase response of the multi-order harmonics of the granules at different frequencies.

While the granular beads show a variety of dynamic nonlinear vibrations, phase difference and the ratio between the amplitudes show a higher field of variation in the nonlinear granules and can be manipulated for the variation of the state of the elastic bit for data information processing.

### **Discussion:**

This study investigates the Berry phase accumulation in a nonlinear granular network by analyzing a theoretical and numerical model and realizing it through experimentation. The study parallels quantum systems by focusing on two-level time-dependent elastic bits. The system's vibration is mapped onto the orthonormal basis through the granules' amplitude and phase. Nonlinearity has opened time-dependent Bloch states, where the orthonormal basis of the coherent states is time-dependent. This allows us to explore the elastic bits in a single excitation rather than the multiple excitations needed for the linearized system. We used a mathematical model to get the multi-order displacement for the granules due to the excitation through the multi-order perturbation method. The perturbation reveals the amplitude, which, with the eigenstates' orthonormal basis, can create time-dependent coherent states by realizing the complex amplitude coefficients  $\tilde{\alpha}$  and  $\tilde{\beta}$ . When the coherent states are mapped onto the Bloch sphere through the polar and azimuthal angle  $\tilde{\theta}$  and  $\tilde{\varphi}$ , we can visualize the evolution of states of the elastic bit of the nonlinear system over time. This allows us to understand the Berry phase of the elastic bit as the frequency can change the Berry phase accumulated in time from trivial to non-trivial. Manipulation is also possible by changing the amplitude of the excitation. The precompression plays a pivotal role as by changing the precompression, we can see the evolution of the Berry phase. With the change of the precompression, the system can be made from highly to weakly nonlinear. The Berry phase change is visualized as a highly nonlinear system that shows multiple non-trivial berry phases along the frequency range. In contrast, the weakly nonlinear system shows a single non-trivial berry phase in the same range. This is due to the linearization of the granular system.

The evolution of the states of the elastic bit can also be matched with the numerical simulations. In a numerical case, multiple orders of amplitude are considered, and we can see the variation in the Berry phase in theoretical and numerical cases. This reveals that the Berry phase of the nonlinear granular network depends on the granules' phase and the granules' amplitude. The ratio between the amplitude of the granules at the characteristic frequencies can affect the Berry phase.

The experimental realization of the two-mass granular system backs the numerical simulation. To analyze the Berry phase through the experimental system, we drive one of the granules and use Poisson's effect to find out the vibrational effect of the granules. Through the span of the frequency, we can see the accumulation of the Berry phase from trivial (0) to non-trivial ( $\pi$ ). If we look at the dynamics of the granules at the specific two points, we can see that the amplitudes and phases at the characteristic frequencies show different amplitudes. Although the driving frequency has similar Berry phases in trivial and non-trivial cases, the frequency of higher-order characteristics varies. This shows that at various driving frequencies, time can have a variety of Berry phase accumulation for the classical system. We also observe the Bloch states, where we can get a higher evolution of the states of the elastic bits over time.

Notably, we have identified the trivial and non-trivial Berry phases under certain scenarios, which can correlate the vibrational effect of the granules with the topological properties of elastic bits. The study demonstrates the possibility of topological quantum computing, where the braiding of two elastic bits utilizes the Berry phase. The time constraint accumulation of the Berry phase lets the global phase take over the information transformation rather than the local perturbation, resulting in a disturbance-free system. This is also important in the Majorana encoding and the field of non-Holonomic computing. This is an innovative and necessary approach to understanding a classical system's bulk edge topological properties. This can help create a decoherence-free data transmission system and design a nonlinearity-based mechanical system.

### **Acknowledgments**

M.A.H. acknowledges partial support from NSF grants 2204382 and 2242925 and thanks Wayne State University Startup Funds for additional support.

### **Author Contributions**

M.A.H. conceived the idea of the research. All authors analyzed the findings and contributed to the scientific discussion and manuscript writings.

### **Competing Interests**

The authors declare no competing interests.

### **Data Availability**

The data that support our findings of the present study are available from the corresponding author upon reasonable request.

## References

1. J W Zwanziger, a. M Koenig, and A. Pines, *Berry's Phase*. Annual Review of Physical Chemistry, 1990. **41**(1): p. 601-646.
2. Berry, M.V., *Quantal phase factors accompanying adiabatic changes*. Proceedings of the Royal Society of London. A. Mathematical and Physical Sciences, 1984. **392**(1802): p. 45-57.
3. Vanderbilt, D., *Berry Phases in Electronic Structure Theory: Electric Polarization, Orbital Magnetization and Topological Insulators*. 2018, Cambridge: Cambridge University Press.
4. Friesen, M., et al., *A decoherence-free subspace in a charge quadrupole qubit*. Nature Communications, 2017. **8**(1): p. 15923.
5. Duan, L.-M. and G.-C. Guo, *Reducing decoherence in quantum-computer memory with all quantum bits coupling to the same environment*. Physical Review A, 1998. **57**(2): p. 737-741.
6. Lidar, D.A., I.L. Chuang, and K.B. Whaley, *Decoherence-Free Subspaces for Quantum Computation*. Physical Review Letters, 1998. **81**(12): p. 2594-2597.
7. Chen, H., H. Nassar, and G.L. Huang, *A study of topological effects in 1D and 2D mechanical lattices*. Journal of the Mechanics and Physics of Solids, 2018. **117**: p. 22-36.
8. Palmer, S.J. and V. Giannini, *Berry bands and pseudo-spin of topological photonic phases*. Physical Review Research, 2021. **3**(2): p. L022013.
9. Bisharat, D., et al., *Photonic Topological Insulators: A Beginner's Introduction [Electromagnetic Perspectives]*. IEEE Antennas and Propagation Magazine, 2021. **63**(3): p. 112-124.
10. Trainiti, G. and M. Ruzzene, *Non-reciprocal elastic wave propagation in spatiotemporal periodic structures*. New Journal of Physics, 2016. **18**(8): p. 083047.
11. Pachos, J. and V. Lahtinen, *A Short Introduction to Topological Quantum Computation*. SciPost Physics, 2017. **3**.
12. Jäck, B., Y. Xie, and A. Yazdani, *Detecting and distinguishing Majorana zero modes with the scanning tunnelling microscope*. Nature Reviews Physics, 2021. **3**(8): p. 541-554.
13. Xu, G.F., et al., *Realizing nonadiabatic holonomic quantum computation beyond the three-level setting*. Physical Review A, 2021. **103**(5): p. 052605.
14. Chen, Z.-G., et al., *Classical non-Abelian braiding of acoustic modes*. Nature Physics, 2022. **18**(2): p. 179-184.
15. Xiao, D., M.-C. Chang, and Q. Niu, *Berry phase effects on electronic properties*. Reviews of Modern Physics, 2010. **82**(3): p. 1959-2007.
16. Deymier, P.A., et al., *Realizing acoustic qubit analogues with nonlinearly tunable phi-bits in externally driven coupled acoustic waveguides*. Scientific Reports, 2023. **13**(1): p. 635.
17. Hasan, M.A., K. Runge, and P.A. Deymier, *Experimental classical entanglement in a 16 acoustic qubit-analogue*. Scientific Reports, 2021. **11**(1): p. 24248.
18. Deymier, P.A., K. Runge, and J.O. Vasseur, *Geometric phase and topology of elastic oscillations and vibrations in model systems: Harmonic oscillator and superlattice*. AIP Advances, 2016. **6**(12).
19. Mahmood, K.T. and M.A. Hasan. *Berry Phase and Topological Insights in a Qubit-Inspired Classical Two-Level Elastic Bit*. 2024.
20. Chen, Y.-F., et al., *Various topological phases and their abnormal effects of topological acoustic metamaterials*. Interdisciplinary Materials, 2023. **2**(2): p. 179-230.

21. Wang, P., L. Lu, and K. Bertoldi, *Topological Phononic Crystals with One-Way Elastic Edge Waves*. Physical Review Letters, 2015. **115**(10): p. 104302.
22. Pal, R.K., et al., *Amplitude-dependent topological edge states in nonlinear phononic lattices*. Physical Review E, 2018. **97**(3): p. 032209.
23. Mahmood, K.T. and M.A. Hasan, *Experimental demonstration of classical analogous time-dependent superposition of states*. Scientific Reports, 2022. **12**(1): p. 22580.
24. Hasan, M.A., et al., *The sound of Bell states*. Communications Physics, 2019. **2**(1): p. 106.
25. Deymier, P.A., et al., *Exponentially Complex "Classically Entangled" States in Arrays of One-Dimensional Nonlinear Elastic Waveguides*. Materials, 2019. **12**(21): p. 3553.
26. Hasan, M.A. and P.A. Deymier, *Modeling and simulations of a nonlinear granular metamaterial: application to geometric phase-based mass sensing*. Modelling and Simulation in Materials Science and Engineering, 2022. **30**(7): p. 074002.
27. Dür, W. and S. Heusler, *What we can learn about quantum physics from a single qubit*. 2013.
28. Nesterenko, V.F., *Dynamics of Heterogeneous Materials*. 2001: Springer.
29. Delplace, P. and A. Venaille, *From the geometry of Foucault pendulum to the topology of planetary waves*. Comptes Rendus. Physique, 2020. **21**(2): p. 165-175.
30. Hasan, M.A., et al., *Spectral analysis of amplitudes and phases of elastic waves: Application to topological elasticity*. The Journal of the Acoustical Society of America, 2019. **146**(1): p. 748-766.
31. Hasan, M.A., et al., *Geometric phase invariance in spatiotemporal modulated elastic system*. Journal of Sound and Vibration, 2019. **459**: p. 114843.
32. Zak, J., *Berry's phase for energy bands in solids*. Physical Review Letters, 1989. **62**(23): p. 2747-2750.
33. Samuel, J. and R. Bhandari, *General Setting for Berry's Phase*. Physical Review Letters, 1988. **60**(23): p. 2339-2342.
34. Raffaele, R., *Manifestations of Berry's phase in molecules and condensed matter*. Journal of Physics: Condensed Matter, 2000. **12**(9): p. R107.
35. Jayaprakash, K.R., et al., *Nonlinear normal modes and band zones in granular chains with no pre-compression*. Nonlinear Dynamics, 2011. **63**(3): p. 359-385.
36. Wallis, R.F., *Theory of Surface Modes of Vibration in Two- and Three-Dimensional Crystal Lattices*. Physical Review, 1959. **116**(2): p. 302-308.
37. Sen, S., et al., *Solitary waves in the granular chain*. Physics Reports-review Section of Physics Letters - PHYS REP-REV SECT PHYS LETT, 2008. **462**: p. 21-66.

### Supplementary Materials:

The general mathematical expression of the two-mass nonlinear granular system, considering the one-dimensional movement of the granules, we get [28],

$$\begin{aligned} m\ddot{u}_1 &= k_{NL}[F_1 \sin(\omega_D t) - u_1 + \delta_0]_+^{\frac{3}{2}} - k_{NL}[u_1 - u_2 + \delta_0]_+^{\frac{3}{2}} - \eta\dot{u}_1 \\ m\ddot{u}_2 &= k_{NL}[u_1 - u_2 + \delta_0]_+^{\frac{3}{2}} - k_{NL}[u_2 - F_2 \sin(\omega_D t) + \delta_0]_+^{\frac{3}{2}} - \eta\dot{u}_2 \end{aligned} \quad (\text{A1})$$

Here,  $u_1$  and  $u_2$  are the displacement of the granules measured from the equilibrium position. In Eq. (1),  $k_{NL}$  is the nonlinear stiffness between the granules and is dependent on the physical properties of the granules ( $k_{NL} = \frac{E\sqrt{2R}}{3(1-\nu^2)}$ ,  $m = \frac{4}{3}\pi R^3$  is the mass of the granules,  $R$  is the radius, and  $\rho$  is the density of the granule material). The damping coefficient  $\eta$  is the dissipation between the granules due to Hertzian contact, and the gravitational effects are neglected. The pre-compression  $\delta_0$  is the static applied load scaled by the radius of the granules. If  $\delta_0 \gg u_1 - u_2$ , using the power expansion through the Taylor series of the nonlinear term, we can get the nonlinear term of the eq. (1) as follows.

$$\begin{aligned} m\ddot{u}_1 &= k_{NL}[F_1 e^{i\omega_D t} - u_1 + \delta_0]_+^{\frac{3}{2}} - k_{NL}[u_1 - u_2 + \delta_0]_+^{\frac{3}{2}} - \eta\dot{u}_1 \\ \Rightarrow m\ddot{u}_1 &= k_{NL}\delta_0^{\frac{3}{2}} \left[ 1 + \frac{F_1 e^{i\omega_D t} - u_1}{\delta_0} \right]_+^{\frac{3}{2}} - k_{NL}\delta_0^{\frac{3}{2}} \left( 1 + \frac{u_1 - u_2}{\delta_0} \right)_+^{\frac{3}{2}} - \eta\dot{u}_1 \\ \Rightarrow m\ddot{u}_1 &= k_{NL}\delta_0^{\frac{3}{2}} \left[ 1 + \frac{3}{2} \left( \frac{F_1 e^{i\omega_D t} - u_1}{\delta_0} \right) - \frac{3}{8} \left( \frac{F_1 e^{i\omega_D t} - u_1}{\delta_0} \right)^2 - \frac{3}{48} \left( \frac{F_1 e^{i\omega_D t} - u_1}{\delta_0} \right)^3 + \dots \right]_+ \\ &\quad - k_{NL}\delta_0^{\frac{3}{2}} \left[ 1 + \frac{3}{2} \left( \frac{u_1 - u_2}{\delta_0} \right) - \frac{3}{8} \left( \frac{u_1 - u_2}{\delta_0} \right)^2 - \frac{3}{48} \left( \frac{u_1 - u_2}{\delta_0} \right)^3 + \dots \right]_+ - \eta\dot{u}_1 \\ \Rightarrow m\ddot{u}_1 &= \left[ \frac{3}{2} k_{NL}\delta_0^{\frac{1}{2}} (F_1 e^{i\omega_D t} - u_1) - \frac{3}{8} k_{NL}\delta_0^{-\frac{1}{2}} (F_1 e^{i\omega_D t} - u_1)^2 - \frac{3}{48} k_{NL}\delta_0^{-\frac{3}{2}} (F_1 e^{i\omega_D t} - u_1)^3 + \dots \right]_+ \\ &\quad - \left[ \frac{3}{2} k_{NL}\delta_0^{\frac{1}{2}} (u_1 - u_2) - \frac{3}{8} k_{NL}\delta_0^{-\frac{1}{2}} (u_1 - u_2)^2 - \frac{3}{48} k_{NL}\delta_0^{-\frac{3}{2}} (u_1 - u_2)^3 + \dots \right]_+ - \eta\dot{u}_1 \\ m\ddot{u}_2 &= -k_{NL}[u_2 - F_2 e^{i\omega_D t} + \delta_0]_+^{\frac{3}{2}} + k_{NL}[u_1 - u_2 + \delta_0]_+^{\frac{3}{2}} - \eta\dot{u}_2 \\ \Rightarrow m\ddot{u}_2 &= -k_{NL}\delta_0^{\frac{3}{2}} \left[ 1 + \frac{u_2 - F_2 e^{i\omega_D t}}{\delta_0} \right]_+^{\frac{3}{2}} + k_{NL}\delta_0^{\frac{3}{2}} \left( 1 + \frac{u_1 - u_2}{\delta_0} \right)_+^{\frac{3}{2}} - \eta\dot{u}_2 \\ \Rightarrow m\ddot{u}_2 &= -k_{NL}\delta_0^{\frac{3}{2}} \left[ 1 + \frac{3}{2} \left( \frac{u_2 - F_2 e^{i\omega_D t}}{\delta_0} \right) - \frac{3}{8} \left( \frac{u_2 - F_2 e^{i\omega_D t}}{\delta_0} \right)^2 - \frac{3}{48} \left( \frac{u_2 - F_2 e^{i\omega_D t}}{\delta_0} \right)^3 + \dots \right]_+ \\ &\quad + k_{NL}\delta_0^{\frac{3}{2}} \left[ 1 + \frac{3}{2} \left( \frac{u_1 - u_2}{\delta_0} \right) - \frac{3}{8} \left( \frac{u_1 - u_2}{\delta_0} \right)^2 - \frac{3}{48} \left( \frac{u_1 - u_2}{\delta_0} \right)^3 + \dots \right]_+ - \eta\dot{u}_2 \\ \Rightarrow m\ddot{u}_2 &= - \left[ \frac{3}{2} k_{NL}\delta_0^{\frac{1}{2}} (u_2 - F_2 e^{i\omega_D t}) - \frac{3}{8} k_{NL}\delta_0^{-\frac{1}{2}} (u_2 - F_2 e^{i\omega_D t})^2 - \frac{3}{48} k_{NL}\delta_0^{-\frac{3}{2}} (u_2 - F_2 e^{i\omega_D t})^3 + \dots \right]_+ \\ &\quad + \left[ \frac{3}{2} k_{NL}\delta_0^{\frac{1}{2}} (u_1 - u_2) - \frac{3}{8} k_{NL}\delta_0^{-\frac{1}{2}} (u_1 - u_2)^2 - \frac{3}{48} k_{NL}\delta_0^{-\frac{3}{2}} (u_1 - u_2)^3 + \dots \right]_+ - \eta\dot{u}_2 \end{aligned} \quad (\text{A2})$$



The simplified nonlinear equations from the Eq. (A2) of the granules can be written as,

$$\begin{aligned}
m\ddot{u}_1 &= \left[ k_1(F_1 e^{i\omega_D t} - u_1) + k_2(F_1 e^{i\omega_D t} - u_1)^2 + k_3(F_1 e^{i\omega_D t} - u_1)^3 + \dots \right]_+ \\
&\quad - \left[ k_1(u_1 - u_2) + k_2(u_1 - u_2)^2 + k_3(u_1 - u_2)^3 + \dots \right]_+ - \eta\dot{u}_1 \\
m\ddot{u}_2 &= - \left[ k_1(u_2 - F_2 e^{i\omega_D t}) + k_2(u_2 - F_2 e^{i\omega_D t})^2 + k_3(u_2 - F_2 e^{i\omega_D t})^3 + \dots \right]_+ \\
&\quad + \left[ k_1(u_1 - u_2) + k_2(u_1 - u_2)^2 + k_3(u_1 - u_2)^3 + \dots \right]_+ - \eta\dot{u}_2
\end{aligned} \tag{A3}$$

Here,  $k_1 = \frac{3}{2}k_{NL}\delta_0^{\frac{1}{2}}$ ,  $k_2 = -\frac{3}{8}k_{NL}\delta_0^{-\frac{1}{2}}$ ,  $k_3 = -\frac{3}{48}k_{NL}\delta_0^{-\frac{3}{2}}$  are the different order coupling stiffness for the granular beads. The solution of the nonlinear system consists of a homogeneous part and a particular part. We apply a particular external force, so the system has one solution since there are no initial conditions. The solution of the system is stated as  $u_1 = u_{1,0} + \epsilon u_{1,1} + \epsilon^2 u_{1,2} + \dots$  and  $u_2 = u_{2,0} + \epsilon u_{2,1} + \epsilon^2 u_{2,2} + \dots$ , which follows the perturbation technique to create an approximate solution of the system. Here,  $\epsilon$  represents the order of the stiffness between the coupling. And  $u_{1,m}$  and  $u_{2,m}$  represents the order of the displacement due to the higher order of stiffness. The system's viscous damping reacts to the movement of the granules, with the adjustment made to the viscous damping due to the drag between the air and the granules.

Using the solution of the displacement  $u_{1,m}$  and  $u_{2,m}$  in the granular network Eq. (2), we get the displacement field as,

Bead 1	$ \begin{aligned} &m(\ddot{u}_{1,0} + \epsilon\ddot{u}_{1,1} + \epsilon^2\ddot{u}_{1,2}) \\ &= k_1[(F_1 e^{i\omega_D t} - u_{1,0}) - (u_{1,0} - u_{2,0})] \\ &+ \epsilon k_2[(-u_{1,1}) - (u_{1,1} - u_{2,1})] + \epsilon^2 k_1[(-u_{1,2}) - (u_{1,2} - u_{2,2})] \\ &+ \epsilon k_2[(F_1 e^{i\omega_D t} - u_{1,0})^2 + \epsilon(-2F_1 e^{i\omega_D t} u_{1,1} + 2u_{1,0} u_{1,1}) \\ &- (u_{1,0} - u_{2,0})^2 \\ &- \epsilon^2(2u_{1,0} u_{1,1} - 2u_{1,1} u_{2,0} - 2u_{1,0} u_{2,1} + 2u_{2,0} u_{2,1})] \\ &+ \epsilon^2 k_3[(F_1 e^{i\omega_D t} - u_{1,0})^3 - (u_{1,0} - u_{2,0})^3] \\ &- \eta(\dot{u}_{1,0} + \epsilon\dot{u}_{1,1} + \epsilon^2\dot{u}_{1,2}) \end{aligned} $	(A4)
Bead 2	$ \begin{aligned} &m(\ddot{u}_{2,0} + \epsilon\ddot{u}_{2,1} + \epsilon^2\ddot{u}_{2,2}) \\ &= k_1[(u_{1,0} - u_{2,0}) - (u_{2,0} - F_2 e^{i\omega_D t})] \\ &+ \epsilon[(u_{1,1} - u_{2,1}) - (u_{2,1})] + \epsilon^2 k_1[(u_{1,2} - u_{2,2}) - (u_{1,2})] \\ &+ \epsilon k_2[-(u_{2,0} - F_2 e^{i\omega_D t})^2 + \epsilon(2F_2 e^{i\omega_D t} u_{2,1} - 2u_{2,0} u_{2,1}) \\ &+ (u_{1,0} - u_{2,0})^2 \\ &+ \epsilon^2(2u_{1,0} u_{1,1} - 2u_{1,1} u_{2,0} - 2u_{1,0} u_{2,1} + 2u_{2,0} u_{2,1})] \\ &+ \epsilon^2 k_3[(u_{1,0} - u_{2,0}) - (u_{2,0} - F_2 e^{i\omega_D t})^3] \\ &- \eta(\dot{u}_{2,0} + \epsilon\dot{u}_{2,1} + \epsilon^2\dot{u}_{2,2}) \end{aligned} $	

By equating coefficient of the order of stiffness, we get multi order displacement field as Eq. (2) and the amplitude response stated as in Eq. (3). This gives us the multi order amplitude  $A_{1,m}$  and  $A_{2,m}$ . The characteristics frequencies and their corresponding amplitudes can be seen in the Fast Fourier Transform of the signal shown in Fig. A1.

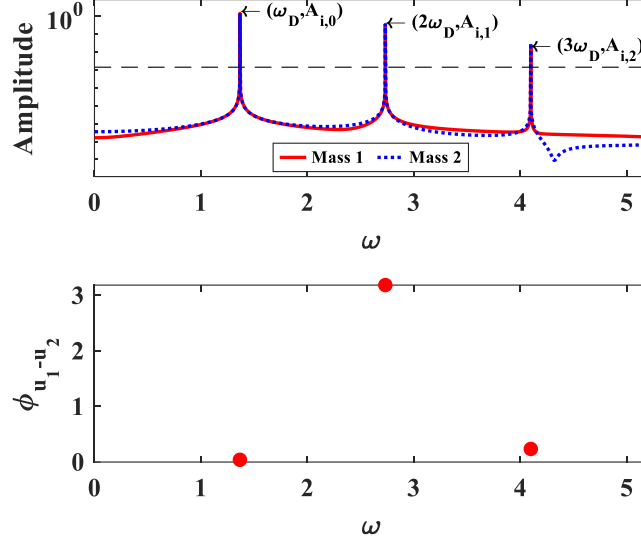


**Figure A1:** Fast Fourier Transform of the nonlinear granular network of Eq. (A4) at a particular driving condition, showcasing the multi order harmonic responses of the granule at the characteristic's frequencies.

In the case of a single amplitude, when the precompression of the system is higher, the system is considered a linearized system because only zeroth order amplitude is present. The vibrational responses of the granules are defined through the eigen states of  $E_1$  and  $E_2$ . As we are using nonlinear system, the total displacement vector for the granule's vibration equation derived through the perturbation theory can be expressed as the sum of the multi-order amplitudes at their characteristics frequencies,

$$\vec{U} = \begin{pmatrix} u_1 \\ u_2 \end{pmatrix} = \sum_{n=1} \begin{pmatrix} \epsilon^{n-1} u_{1,n-1} \\ \epsilon^{n-1} u_{2,n-1} \end{pmatrix} = \sum_{n=1} \begin{pmatrix} A_{1,n-1} \\ A_{2,n-1} \end{pmatrix} e^{ni\omega_n t} \quad (\text{A5})$$

The combinations of  $E_1$  and  $E_2$  form a complete orthonormal basis for the granular network despite the absence of the orthogonality property of the nonlinear modes in the Hilber space. For each of the characteristic's frequencies, we can write the amplitude as,

$$\begin{pmatrix} A_{1,n-1} \\ A_{2,n-1} \end{pmatrix} e^{ni\omega_n t} \equiv \frac{1}{\sqrt{|\alpha_n|^2 + |\beta_n|^2}} (\alpha_n E_1 + \beta_n E_2) e^{i\omega_n t} \quad (\text{A6})$$

Here,  $\alpha_n$  and  $\beta_n$  are the complex amplitude coefficients stating the orthonormal basis at the characteristic frequency of the displacement field. And  $n = 1, 2, \dots$  are the  $n^{\text{th}}$  complex amplitudes of the  $n^{\text{th}}$  dominant characteristic frequency.  $\alpha_n$  and  $\beta_n$  are dependent on each other through phase and form a coherent superposition of states in the form of two possible vibration modes. Therefore, we use the analogy of the quantum system, Dirac notations for vectors, and apply them to the elastic states in Eq. (A6). Hence, the total displacement field has a complex time-dependent coefficient.  $\tilde{\alpha}(t)$  and  $\tilde{\beta}(t)$ , which can be expressed as,

$$\begin{aligned} \vec{U} &= \begin{pmatrix} A_{1,0} \\ A_{2,0} \end{pmatrix} e^{i\omega_1 t} + \begin{pmatrix} A_{1,1} \\ A_{2,1} \end{pmatrix} e^{2i\omega_2 t} + \begin{pmatrix} A_{1,2} \\ A_{2,2} \end{pmatrix} e^{3i\omega_3 t} \\ &\equiv (\alpha_1 |E_1\rangle + \beta_1 |E_2\rangle) e^{i\omega_1 t} + (\alpha_2 |E_1\rangle + \beta_2 |E_2\rangle) e^{2i\omega_2 t} \\ &\quad + (\alpha_3 |E_1\rangle + \beta_3 |E_2\rangle) e^{3i\omega_3 t} \end{aligned} \quad (\text{A7})$$

$$\begin{aligned}
\Rightarrow \vec{U} &= \sum_n \begin{pmatrix} A_{1,n} \\ A_{2,n} \end{pmatrix} e^{ni\omega_n t} \\
&\equiv (\alpha_1 e^{i\omega_1 t} |E_1\rangle + \beta_1 e^{i\omega_1 t} |E_2\rangle) + (\alpha_2 e^{2i\omega_2 t} |E_1\rangle + \beta_2 e^{2i\omega_2 t} |E_2\rangle) \\
&\quad + (\alpha_3 e^{3i\omega_3 t} |E_1\rangle + \beta_3 e^{3i\omega_3 t} |E_2\rangle) \\
\Rightarrow \vec{U} &= \sum_n \begin{pmatrix} A_{1,n} \\ A_{2,n} \end{pmatrix} e^{ni\omega_n t} \\
&\equiv (\tilde{\alpha}_1(t) |E_1\rangle + \tilde{\beta}_1(t) |E_2\rangle) + (\tilde{\alpha}_2(t) |E_1\rangle + \tilde{\beta}_2(t) |E_2\rangle) \\
&\quad + (\tilde{\alpha}_3(t) |E_1\rangle + \tilde{\beta}_3(t) |E_2\rangle) \\
\Rightarrow \vec{U} &= \sum_n \begin{pmatrix} A_{1,n} \\ A_{2,n} \end{pmatrix} e^{ni\omega_n t} \\
&\equiv [\tilde{\alpha}_1(t) + \tilde{\alpha}_2(t) + \tilde{\alpha}_3(t)] |E_1\rangle + [\tilde{\beta}_1(t) + \tilde{\beta}_2(t) + \tilde{\beta}_3(t)] |E_2\rangle \\
\Rightarrow \vec{U} &= \sum_n \begin{pmatrix} A_{1,n} \\ A_{2,n} \end{pmatrix} e^{ni\omega_n t} \equiv \frac{1}{\sqrt{|\tilde{\alpha}(t)|^2 + |\tilde{\beta}(t)|^2}} [\tilde{\alpha}(t) |E_1\rangle + \tilde{\beta}(t) |E_2\rangle]
\end{aligned}$$

This allows the coherent states coefficient to become time-dependent, as the multiple characteristics frequency allows time to evolve in the Hilbert space. This coherent time-dependent superposition of states can be visualized in a 3-dimensional geometric space through geometrical representation of Bloch sphere. The Bloch sphere has two components: polar angle  $\theta$  and azimuthal angle  $\varphi$ . The components are also time-dependent ( $\tilde{\theta}$  and  $\tilde{\varphi}$ ), as the coefficients are time dependent. We can get from Eq. (A7) as,

$$\begin{aligned}
\vec{U} &= \tilde{\alpha} |E_1\rangle + \tilde{\beta} |E_2\rangle \\
\Rightarrow \vec{U} &= \tilde{r}_\alpha e^{i\tilde{\xi}_\alpha} |E_1\rangle + \tilde{r}_\beta e^{i\tilde{\xi}_\beta} |E_2\rangle
\end{aligned} \tag{A8}$$

Here  $\tilde{r}_\alpha$  and  $\tilde{r}_\beta$  are the modulus of the complex amplitude coefficients of  $\tilde{\alpha}$  and  $\tilde{\beta}$ . the superposition of states are represented in a polar space as  $\tilde{r}_\alpha = \cos \tilde{\theta}$  and  $\tilde{r}_\beta = \sin \tilde{\theta}$ , where  $\tilde{\theta}$  is the angle of the superposition of states with the z axis of a Bloch sphere shown in Fig. A2 [R1].

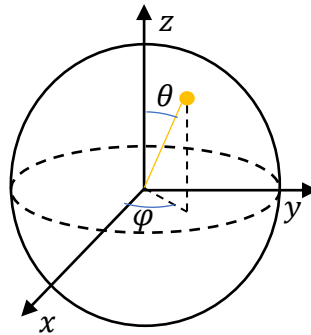


**Figure A2:** 3D sphere depicting the Bloch sphere and the corresponding angles with the cartesian axis of the sphere. It demonstrates the elastic bit state through sphere's axes and the defining angles-  $\tilde{\theta}$  and  $\tilde{\varphi}$ .

In Fig. A2, the z axis in a Bloch sphere represents the pure states  $|E_1\rangle$  and  $|E_2\rangle$  and referred as polar angle. We multiply both sides of Eq. (A10) by a variable of the global phase  $e^{-i\tilde{\xi}_\alpha}$ . Global phase is the overall phase difference in a quantum system where this relative phase does not affect the observable properties of that system. Applying the global phase in the displacement field of Eq. (A8), we get  $\vec{U}' = e^{-i\tilde{\xi}_\alpha}\vec{U}$ . And the state space of the granular network is represented as,

$$\begin{aligned}\vec{U}' &= \tilde{r}_\alpha |E_1\rangle + \tilde{r}_\beta e^{i(\tilde{\xi}_\beta - \tilde{\xi}_\alpha)} |E_2\rangle \\ \vec{U}' &= \cos \tilde{\theta} |E_1\rangle + \sin \tilde{\theta} e^{i\tilde{\varphi}} |E_2\rangle\end{aligned}\quad (\text{A9})$$

So, the phase difference between the complex amplitude coefficients is referred as azimuthal angle  $\tilde{\varphi} = \tilde{\xi}_\beta - \tilde{\xi}_\alpha$ .  $\tilde{\varphi}$  represents the rotation of the states in the x-y plane stated in Fig. A2. To restrict the ranges of both angles, we use half angle of polar angle  $\tilde{\theta}$  to represent the state on the Bloch sphere. As the global phase does not create change in the superposition of states, we can find the displacement field as,

$$\vec{U} = \cos \frac{\tilde{\theta}}{2} |E_1\rangle + e^{i\tilde{\varphi}} \sin \frac{\tilde{\theta}}{2} |E_2\rangle \quad (\text{A10})$$

Where,  $0 \leq \theta \leq \pi$  and  $0 \leq \varphi \leq 2\pi$

The phase difference of the coherent states forms the rotation of the states in the Bloch sphere, which is the azimuthal angle  $\tilde{\varphi}$ . So, the mapping of the coherent states in the Bloch sphere is defined as,

$$\tilde{\theta}(t) = 2 \cos^{-1}(|\tilde{\alpha}(t)|), \tilde{\varphi}(t) = \arg(\tilde{\alpha}(t)) - \arg(\tilde{\beta}(t)) \quad (\text{A11})$$

The Bloch sphere represents the linear combination of  $E_1$  and  $E_2$  and the superposition of states depends on  $\theta$  and  $\varphi$ . Hence, the Bloch sphere also represents the orthogonal eigenstates that depend on  $\tilde{\theta}(t)$  and  $\tilde{\varphi}(t)$  as  $\tilde{\alpha}(t)$  and  $\tilde{\beta}(t)$ . The modal contribution to the overall displacement field's mode superposition can be expressed as a column displacement vector.  $|\psi\rangle$ .

$$|\psi\rangle = \begin{pmatrix} \sum_n \frac{1}{\sqrt{|\alpha_n|^2 + |\beta_n|^2}} \alpha_n e^{ni\omega_n t} \\ \sum_n \frac{1}{\sqrt{|\alpha_n|^2 + |\beta_n|^2}} \beta_n e^{ni\omega_n t} \end{pmatrix} = \begin{pmatrix} \tilde{\alpha}(t) \\ \tilde{\beta}(t) \end{pmatrix} = \begin{pmatrix} \cos \frac{\tilde{\theta}(t)}{2} \\ e^{i\tilde{\varphi}(t)} \sin \frac{\tilde{\theta}(t)}{2} \end{pmatrix} \quad (\text{A12})$$

### PROCEDURE FOR CONDUCTING THE EXPERIMENT:

As the theoretical and numerical background of the nonlinear granular system is set, we create an experimental setup to observe the evolution of the Bloch states and the accumulation of the Berry phase. The experimental setup consists of elastic granular beads with single-point contact and are driven harmonically. The soft plastic material acting as a vise jaw applies a precompression that reduces vibrational transmissions. The external driving frequency ( $\omega_D$ ), the frequency is swept from a lower value of 2 kHz to a higher value of 8 kHz with an increment of 100 Hz at a fixed voltage amplitude of  $120V_{p-p}$ . The highly nonlinear granular beads (52100 Alloy Steel: McMaster-Carr 9528K33, 1-inch diameter, Young's Modulus 210 GPa, density 7810 kg/m<sup>3</sup>) are adaptable to different frequencies and amplitudes. The system was driven by a single transducer (V133-RM Olympus IMS) at one end. The transducer is driven through an amplifier (PD200 60W high bandwidth, low noise linear amplifier) and coupled with a waveform generator (B&K Precision 4055B). Three similar transducers are used to record the responses. One record

transducer is placed in the longitudinal direction, and two record transducers are placed in the lateral direction. The signal responses from the three recording transducers are measured through the oscilloscope (Tektronix MDO3024 Mixed Domain Oscilloscope) and averaged across 512-time series to minimize recording error. The generation of the varying frequency and amplitude and the recording of the signals and data are controlled and processed by MATLAB-based custom algorithms. Uniform compression force  $F_0$  is provided in both ends of the system using a bench vise to fix the initial displacement  $\delta_0$  between the granules centers. The responses are obtained from the lateral detecting transducers of the granules at a steady state. The alignment of the granules is center to center and guaranteed to the limit of human eye precision. Mechanical disturbance can occur in the system due to the natural frequency of the vise holding the setup. We processed the data for the sampling frequency of 999.89 kHz, and considering the noises occurring from the environment, the data are filtered by a low pass frequency of 175 kHz. The resultant signal is processed till 25 kHz to get the pure response of the signal data. This can be implemented to get the current system's signal-to-noise ratio (SNR). The signal-to-noise ratio (SNR) is a measure used to quantify the quality of a signal in the presence of noise [R2]. In acoustics, it represents the ratio of the signal's power to the noise's power.

### Supplementary Reference

- R1. Oliveira, I.S., et al., 3 - *Fundamentals of Quantum Computation and Quantum Information*, in *NMR Quantum Information Processing*, I.S. Oliveira, et al., Editors. 2007, Elsevier Science B.V.: Amsterdam. p. 93-136.
- R2. Welvaert, M. and Y. Rosseel, *On the Definition of Signal-To-Noise Ratio and Contrast-To-Noise Ratio for fMRI Data*. PLOS ONE, 2013. **8**(11): p. e77089.